

Review

# Research on Mid-Infrared External Cavity Quantum Cascade Lasers and Applications

Yuhang Ma, Keke Ding, Long Wei, Xuan Li , Junce Shi, Zaijin Li \*, Yi Qu, Lin Li, Zhongliang Qiao , Guojun Liu, Lina Zeng and Dongxin Xu

Key Laboratory of Laser Technology and Optoelectronic Functional Materials of Hainan Province, Academician Team Innovation Center of Hainan Province, College of Physics and Electronic Engineering, Hainan Normal University, Haikou 571158, China

\* Correspondence: lizaijin@126.com

**Abstract:** In this paper, we review the progress of the development and application of external cavity quantum cascade lasers (ECQCLs). We concentrated on ECQCLs based on the wide tunable range for multi-component detection and applications. ECQCLs in the mid-infrared band have a series of unique spectral properties, which can be widely used in spectroscopy, gas detection, protein detection, medical diagnosis, free space optical communication, and so on, especially wide tuning range, the tuning range up to hundreds of wavenumbers; therefore, ECQCLs show great applications potential in many fields. In this paper, the main external cavity structures of ECQCLs are reviewed and compared, such as the Littrow structure, the Littman structure, and some new structures. Some new structures include the intra-cavity out-coupling structure, multimode interference (MMI) structure, and acousto-optic modulator (AOM) control structure. At the same time, the application research of ECQCLs in gas detection, protein detection, and industry detection are introduced in detail. The results show that the use of diffraction gratings as optical feedback elements can not only achieve wide tuning, but it also has low cost, which is beneficial to reduce the complexity of the laser structure. Therefore, the use of diffraction gratings as optical feedback elements is still the mainstream direction of ECQCLs, and ECQCLs offer a further new option for multi-component detection.

**Keywords:** detection; ECQCL; QCL; tunable



**Citation:** Ma, Y.; Ding, K.; Wei, L.; Li, X.; Shi, J.; Li, Z.; Qu, Y.; Li, L.; Qiao, Z.; Liu, G.; et al. Research on Mid-Infrared External Cavity Quantum Cascade Lasers and Applications. *Crystals* **2022**, *12*, 1564. <https://doi.org/10.3390/cryst12111564>

Academic Editors: Ludmila Isaenko, Yongyi Chen and Li Qin

Received: 14 September 2022

Accepted: 1 November 2022

Published: 2 November 2022

**Publisher's Note:** MDPI stays neutral with regard to jurisdictional claims in published maps and institutional affiliations.



**Copyright:** © 2022 by the authors. Licensee MDPI, Basel, Switzerland. This article is an open access article distributed under the terms and conditions of the Creative Commons Attribution (CC BY) license (<https://creativecommons.org/licenses/by/4.0/>).

## 1. Introduction

The operating wavelength of III-V PN junction semiconductor lasers based on quantum wells usually does not exceed 4  $\mu\text{m}$ , which cannot meet the wavelength requirements of mid-far-infrared. Due to the existence of manufacturing defects, coupled with excessive Auger recombination loss and free carrier absorption loss, the high-quality operation of the laser cannot be guaranteed. The mid-infrared laser with a wide tunable wavelength can be produced by using nonlinear optical phenomena, which originates from the nonlinear polarizability of material. The optical parametric oscillator (OPO) is a typical example of using difference frequency generation (DFG), and it can generate a mid-infrared laser with the frequency by combining a near-infrared laser with a visible laser. The major advantage of OPO systems is their good accessibility to various pulse forms. By using an ultra-short pulse laser in femtosecond scale, it is possible to generate an extremely strong peak power of up to several MW in pulse mode. Such features are quite advantageous for nonlinear microscopy applications. However, the drawback of OPO systems is their less robustness due to its complex optical system, and the tuning range is still limited because of the wavelength accessibility of nonlinear crystals. In addition, the OPO needs a pump laser system for the optical pumping to generate the nonlinear optical process. Thus, the final form of the whole system is inevitably large and not suitable as a portable system. Distributed feedback (DFB) lasers can also generate mid-infrared wavelength and are very useful for spectroscopic sources,

but their main disadvantages are their limited tuning capability and lower output power. In order to meet the needs of mid-far-infrared wavelengths, a new type of infrared laser is required, and QCLs are a good choice, which utilize electronic transitions between quantum well subbands instead of interband optical transitions.

The emergence of QCL has created a precedent for the development of mid-far-infrared semiconductor lasers using wide-bandgap materials. Due to its narrow linewidth and high-power operation in the mid-infrared band (3–24  $\mu\text{m}$ ) at room temperature continuous wave (CW) conditions, it is very suitable for tracing gas sensing in mid-infrared spectroscopy. At present, quantum well lasers in the mid-infrared band lack continuous wave tunability. Gas lasers, such as CO lasers and CO<sub>2</sub> lasers, have a large volume and weight. Lead salt semiconductor lasers have high cooling requirements and low output laser power. QCL overcomes these shortcomings; thus, it can be used in directional infrared countermeasure, gas pollution detection, medical diagnosis, etc. ECQCLs can broaden the working wavelength, improve the beam quality and output laser power, and promote the applications of QCLs.

## 2. ECQCLs Basic Structure and Characteristics

### 2.1. Basic Structure of ECQCLs

In general, mid-infrared semiconductor lasers without any other lasers are compact and easy to use; however, their performance is limited because the emission wavelength is not a single laser mode, but it often has multiple laser modes in the spectrum. In addition, the linewidth of each mode is not narrow enough. Therefore, a form of Fabry-Perot (FP) laser is not suitable for spectroscopy applications. An ECQCL is a wavelength tunable laser, which includes an optical gain medium, an optical device for coupling the output of the gain dielectric waveguide to the free space mode of the external cavity, and a wavelength selective component, such as an interference filter or diffraction grating. Other additional optics such as polarizers, beam splitters, and prisms can also be integrated. Compared with FP lasers, ECQCL does not only benefit the tunability, but it also greatly improves the linewidth of the laser.

The basic structure of ECQCLs is usually composed of a laser external cavity and optical feedback elements, such as collimating lenses and wavelength selectors. The wavelength selectors can be a diffraction grating, a photoelectric filter, an acousto-optic filter, etc., and the laser is enhanced through the feedback of the selectors. The spectrum can be reflected by rotating the angle of the grating; thereby, the laser emission wavelength can be adjusted. The basic structure of an ECQCL is shown in Figure 1.

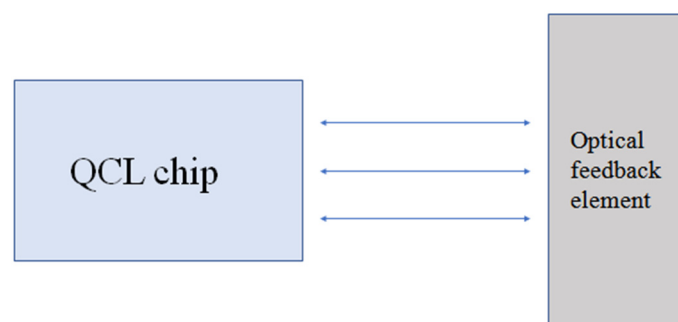


**Figure 1.** Basic structure of ECQCLs.

### 2.2. Operating Principle of QCLs

QCL is a unipolar semiconductor device that utilizes electron transitions between the subbands confined in the heterostructure conduction band for light emission. The electron distribution of a QCL needs to be designed to have a population inversion by adjusting the thicknesses of quantum wells and barriers. Injected electrons flow from the upper levels to lower levels by following the sequential wavefunctions, which represents the electron probability. During this process, the electrons optically transit at the “active region”. By

piling the active region of the same design in sequence, light emission can be amplified. As a consequence, the light emitted from one active region stimulates the following radiation of photons, achieving laser oscillation. During this process, the electrons flow through from one active region to the next active region while generating the stimulated emission of photons and electrons. This is why the laser device is called a quantum “cascade” laser. The more cascades are built, the more electrons can contribute to the stream for light emission. This optical amplification mechanism gives higher quantum efficiency in the laser operation.

QCLs avoid the operating principle of conventional semiconductor lasers by relying on a radically different process for laser emission, which is independent of the band gap [1]. Instead of using opposite charge carriers in semiconductors (electrons and holes) at the bottom of their respective conduction bands and valence bands, which recombine to produce light of frequency  $\nu \approx E_g/h$  (where  $E_g$  is the energy band gap and  $h$  is Planck’s constant), QCLs use only one type of charge carriers (electrons), which undergo a quantum jump between energy levels  $E_n$  and  $E_{n-1}$  to create a laser photon of frequency  $(E_n - E_{n-1})/h$ . The energy diagram of QCLs is shown in Figure 2. These energy levels do not naturally exist in the constituent materials of the active region, but they are artificially created by constructing the active region into nanometer-thick quantum wells. The electron motion perpendicular to the layer interface is quantized and characterized in terms of energy levels, the difference of which is determined by the thickness of the wells and the height of the energy barrier separating the wells. The implications of this new approach are profound. Based on the decoupling of lasing emissions from the bandgap by exploiting optical transitions between quantized electronic states, QCLs are equivalent to a laser with operating characteristics that are quite different from semiconductor lasers and features far superior to semiconductor lasers.

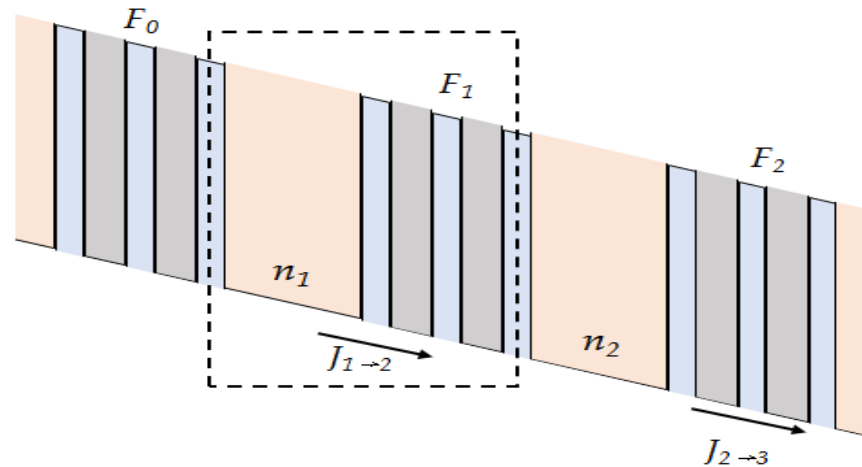


**Figure 2.** Energy diagram of three well structures of QCL (current densities  $J_m$ , electron densities  $n_m$  and fields  $F_m$ , module number  $m$ ).

### 3. Research Progress of ECQCLs

The structures of ECQCLs can be mainly divided into the Littrow structure, the Littman structure, and some new structures. Some new structures include the intra-cavity out-coupling structure, the MMI structure, and the AOM control structure. This paper mainly discusses the research progress of the Littrow structure, the Littman structure, and some new structures of ECQCLs.

#### 3.1. Littrow Structure of ECQCLs

The Littrow structure of ECQCLs is composed of a QCL gain chip, a collimating lens, and a diffraction grating, as shown in Figure 3. The QCL emits from the front end of the gain chip, then enters the diffraction grating for diffraction after collimating the beam

through the collimating lens. The first-order diffraction laser returns to the gain chip along the original optical path, and the laser is output from the zero-order diffraction direction of the grating or the rear end of the gain chip.

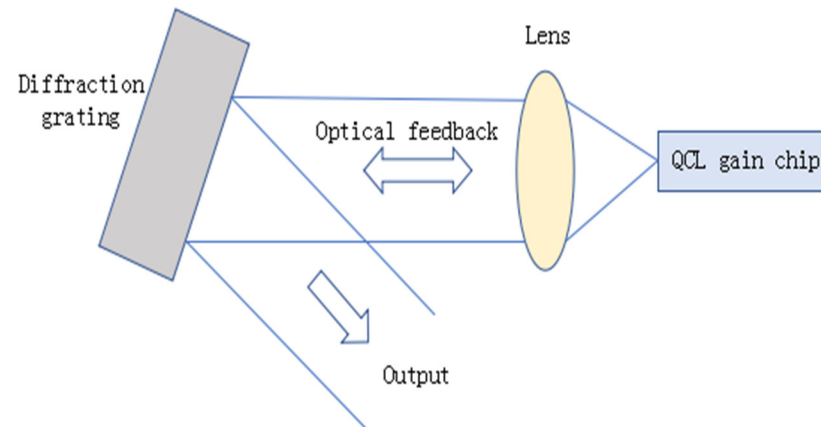


**Figure 3.** Littrow structure of ECQCL.

In 2006, R Maulini et al. [2] reported an ECQCL that was tuned from 8.2  $\mu\text{m}$  to 10.4  $\mu\text{m}$ . The ECQCL was operated in pulse mode at room temperature. For achieving tunability, the laser beam was collimated using an aspheric germanium lens and a blazed grating mounted in the Littrow structure to provide optical feedback. The zero-order reflection laser was output from the grating. The ECQCL was operated in pulse mode by using 100 ns pulse with a repetition rate of 200 kHz.

In 2009, Wysocki Gerard et al. [3] reported broadband mid-infrared laser heterodyne radiation measurements using an ECQCL. The ECQCL was operated at 8.4  $\mu\text{m}$  and was able to provide tunability up to 180  $\text{cm}^{-1}$  at  $-30\text{ }^\circ\text{C}$ .

In 2014, M. Carras et al. [4] reported a 7.5  $\mu\text{m}$  ECQCL spectrometer. The laser used in the spectrometer was an ECQCL. The ECQCL system used the Littrow structure, which consisted of only two optical elements, a lens for laser collimation and a diffraction grating. Rotating the diffraction grating by  $1.75^\circ$ , the laser achieved a tuning range of 57  $\text{cm}^{-1}$  in a single mode emission wavelength from 7.4  $\mu\text{m}$  to 7.73  $\mu\text{m}$ . The wide tuning range was to be achieved over 60.4  $\text{cm}^{-1}$ .

In 2015, Feng Xie et al. [5] reported an ultra broad tunable QCL array in the Littrow structure; the wavelength tunable range was from 6.5 to 10.4  $\mu\text{m}$ , the SMSR showed 20–25 dB, and the threshold current showed 1.7–3.9  $\text{kA}/\text{cm}^2$ .

In 2016, Zhibin Zhao et al. [6] reported a tunable ECQCL with a 7.2  $\mu\text{m}$  central wavelength that was operated at room temperature. The ECQCL was implemented in a Littrow structure. The backside of the gain chip had a highly reflective coating. A two-layer anti-reflection (AR) coating composed of  $\text{Al}_2\text{O}_3$  and ZnSe was deposited on the front side of the chip to suppress the FP mode. By using this AR coating, the single-mode tuning range of the ECQCL was reached at 128  $\text{cm}^{-1}$ , and the wavelength was from 6.78  $\mu\text{m}$  to 7.43  $\mu\text{m}$ . A high SMSR was over 30 dB, and an ultra-low threshold current density was 0.89  $\text{kA}/\text{cm}^2$ . The ECQCL was operated in CW mode at 20  $^\circ\text{C}$ , and an output power of 50 mW was obtained.

In 2022, Ismail Bayrakli [7] reported an ECQCL that used an FP QCL without an antireflection facet coating on the gain chip in the Littrow structure. In addition to electrical pumping, a DFB QCL was also used to optically pump the FP QCL. The spectral range was from 4.45  $\mu\text{m}$  to 4.8  $\mu\text{m}$ , and a wide-range dual-mode tuning range of 164  $\text{cm}^{-1}$  was achieved.

In 2022, Ismail Bayrakli [8] reported two tunable ECQCLs that used intra-cavity and extra-cavity acousto-optic frequency shifters (AOFS), respectively. In the extra-cavity AOFS structure, the wide coarse tunable range was 256  $\text{cm}^{-1}$ , the wavelength range was between 4.33  $\mu\text{m}$  and 4.87  $\mu\text{m}$ , and the fine tunable range was 0.3  $\text{cm}^{-1}$ ; it obtained within 6 ms by

adjusting the injected current. In the intra-cavity AOFS structure, the wavelength was tuned rapidly at  $50 \mu\text{s}$  over a broad tunable bandwidth of  $33 \text{ cm}^{-1}$  by changing the frequency of the AOF from 65 MHz to 89 MHz. The structures are shown in Figure 4.

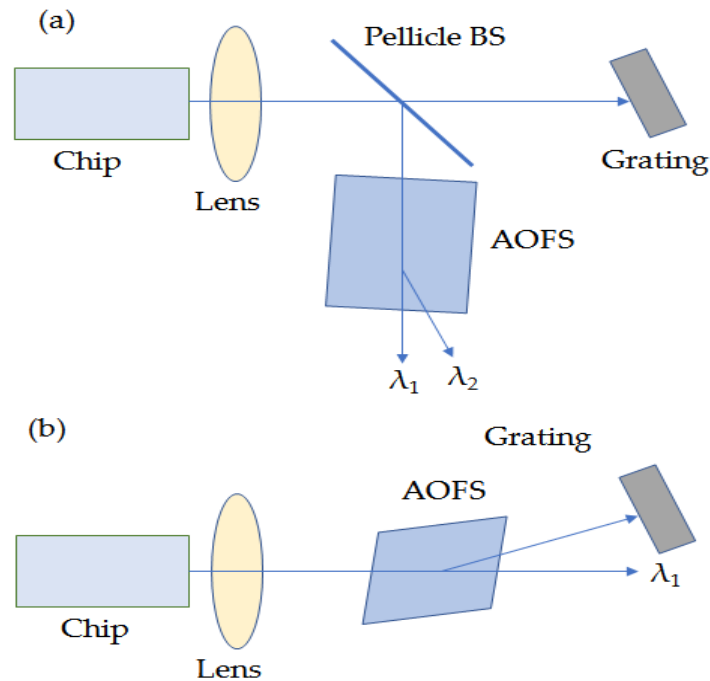


**Figure 4.** Two tunable structures of ECQCL: (a) ECQCL with extra-cavity AOFS, (b) ECQCL with intra-cavity AOFS. BS: Beam splitter.

### 3.2. Littman Structure of ECQCLs

The Littman structure added a mirror to the Littrow structure, and the Littman structure is shown in Figure 5. The first-order diffracted laser is reflected by the mirror and diffracted for the second time, and then it is fed back to the QCL gain chip and forms a resonance. Through mode competition, the first-order diffraction mode is amplified, other oscillation modes are suppressed, and the laser achieves single-mode output.

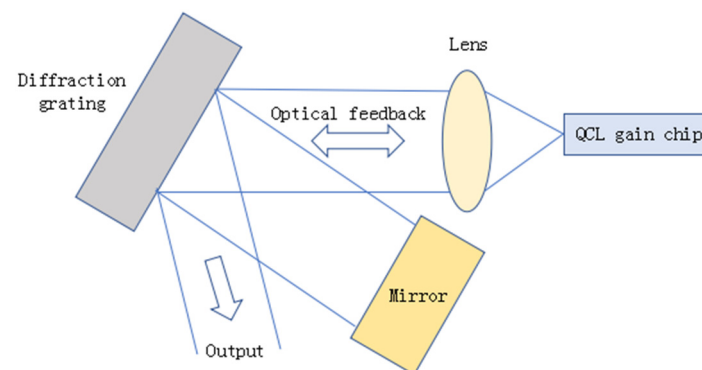


**Figure 5.** Littman structure of ECQCL.

In 2002, Guipeng Luo et al. [9] reported a Littman–Metcalf structure ECQCL; the operating wavelength of the ECQCL was  $5.1 \mu\text{m}$ , and the wavelength tunable range was 245 nm for temperatures from 80 to 243 K.

In 2016, Wei Luo et al. [10] reported an ECQCL that used a Littman–Metcalf structure; the operating wavelength of the ECQCL was  $6.9 \mu\text{m}$ , and the tunable range was from 1340 to  $1640 \text{ cm}^{-1}$ .

In 2018, Xuefeng Jia et al. [11] reported a low threshold current and fast wavelength tunable ECQCL that used a scanning galvanometer in the Littman-Metcalf cavity structure. The ECQCL was scanned repeatedly at 100 Hz over a full tunable range of about 290 nm, from 4.46  $\mu\text{m}$  to 4.75  $\mu\text{m}$ , by providing a scan speed of 59.3  $\mu\text{m}/\text{s}$ . The CW mode threshold current of ECQCL was as low as 250 mA for a 3 mm long QCL gain chip, and the maximum output power was 20.8 mW at 400 mA.

In 2018, Tatsuo Dougakiuchi et al. [12] reported an ECQCL based on the Littman structure. The tunable range was from 895  $\text{cm}^{-1}$  to 990  $\text{cm}^{-1}$ , and the output power of the ECQCL for a tunable wavelength was about 8 mW.

A Littrow structure ECQCL is usually composed of a QCL gain chip, an optical lens, and a diffraction grating. By changing the grating angle, the light wave of a certain wavelength is fed back to the QCL gain chip, which greatly increases the diffraction loss of the light wave of other wavelengths. At the same time, the overall length of the resonator is changed, and a narrow linewidth laser output with a stable wavelength is realized. A Littman structure ECQCL is usually composed of a QCL gain chip, an optical lens, a diffraction grating, and a mirror. The mirror acts as a tuner, the grating is fixed, and the incident light is returned along the incident light path by changing the angle of the mirror. After the light wave is second diffracted by the grating, the SMSR is greatly improved and the laser linewidth is further narrowed. However, its structure is more complex than a Littrow structure ECQCL, resulting in a large power loss. It is not easy to achieve high power output.

### 3.3. New Structures of ECQCLs

An intra-cavity out-coupling structure is a new optical structure for further improvement performances of ECQCL. By placing a BS inside the laser external cavity, much more power was directly extracted from the structure. The structure is shown in Figure 6.

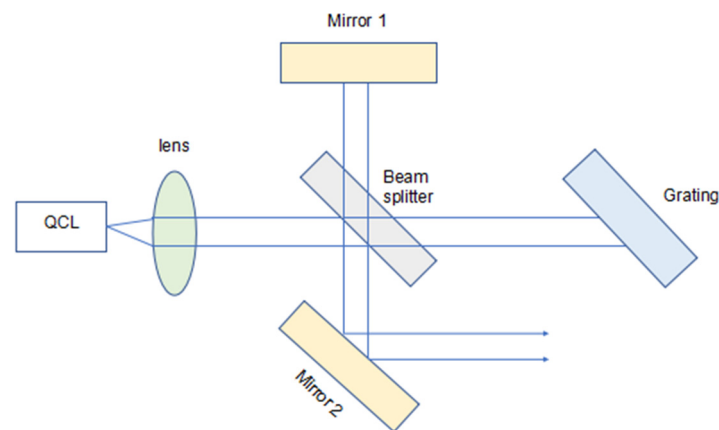


**Figure 6.** Intra-cavity out-coupling structure of ECQCL.

In 2018, Yohei Matsuoka et al. [13] reported an ECQCL with an intra-cavity out-coupling structure that can be tuned from 8.4  $\mu\text{m}$  to 10.8  $\mu\text{m}$ . Compared to the conventional Littrow structure of ECQCLs, this structure achieved higher output power and maintained a broad wavelength tunability. The maximum output power was 1 W in pulsed mode, which was more than double the output power of the Littrow structure using the same QCL gain chip.

For a single-mode laser, an excellent choice for beam splitting is the MMI [14,15], which has long been used for near-infrared beam splitting, with high splitting efficiency. The MMI structure of an ECQCL is shown in Figure 7. The MMI QCL array is collimated by collimating lens. The collimated beam is diffracted on the grating. The first-order diffracted beam is fed back to the MMI QCL array for mode selection. Wavelength tuning is achieved by changing the placement angle of the grating.

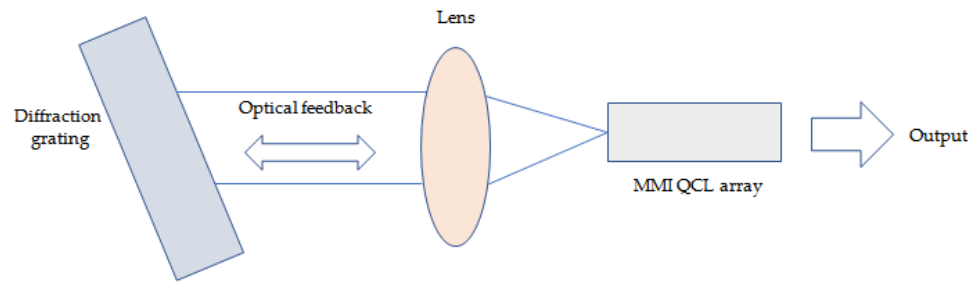


**Figure 7.** MMI structure of an ECQCL.

In 2021, Zeng-Hui Gu et al. [16] reported an MMI structure of an ECQCL that was designed to simplify the fabrication of QCL arrays. A wavelength tuning range of more than  $60 \text{ cm}^{-1}$  was demonstrated, and the ECQCL realized a high power and frequency tunable.

The main disadvantage of a mechanically controlled grating-based ECQCL is the relatively slow wavelength tuning, typically tens of milliseconds. Combustion and explosion diagnostics and some other infrared national defense applications require fast tuning over a broad mid-infrared range. Compared to conventional ECQCLs with mechanically controlled gratings, the use of an electrically controlled AOM enables fast wavelength tuning. In an AOM, radio-frequency acoustic waves are produced by applying an electronic signal to a piezoelectric transducer connected to an optical crystal, such as germanium, that is transparent at the wavelengths the laser needs to operate. The acoustic wave represents the phase transmission grating from which the light beam passing through the AOM crystal can be diffracted.

In 2019, Arkadiy Lyakh et al. [17] reported a new structure that combined AOM tuning with heterogeneous QCL, with the goal of developing a laser source for ultrafast tuning in a broad infrared spectral region. The tunable range of the laser was from  $1990 \text{ cm}^{-1}$  to  $2250 \text{ cm}^{-1}$ , and the schematic diagram is shown in Figure 8.

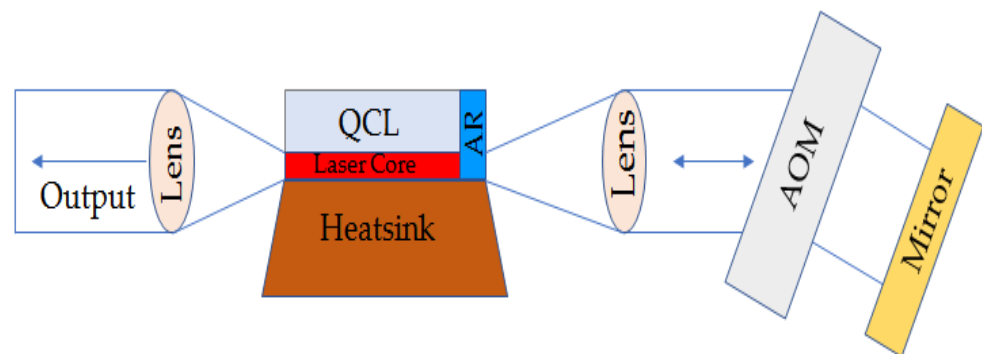


**Figure 8.** Structure of an AOM-controlled ECQCL.

The research development on performances of ECQCLs in recent years is listed in Table 1. Compared with the Littrow structure of ECQCLs, the Littman structure of ECQCLs and some new structures of ECQCLs have the characteristic of a wide tunable range, and they can be widely used in various fields. By changing the optical feedback elements, a wider wavelength tuning range and a higher power are realized. Therefore, some new optical feed elements or new structures can make the ECQCLs obtain a wider wavelength tunable range, a higher power, and a higher SMSR.

**Table 1.** The performance parameters of ECQCLs in recent years.

Type	$\lambda$ ( $\mu\text{m}$ )	Tunable Range ( $\mu\text{m}$ )	Output Power (mW)	SMSR (dB)	Resolution ( $\text{cm}^{-1}$ )	Year
Littman	5.1	0.245	10	40	0.062	2002 [9]
Littrow	8.2–10.4	2.2 *	147	30	-	2006 [2]
Littrow	8.4	0.352 *	>50	-	0.001	2009 [3]
Littrow	7.5	0.33 *	73	-	0.36	2014 [4]
Littrow	6.5–10.4	3.9	250	25	-	2015 [5]
Littrow	6.78–7.43	0.65 *	50	30	-	2016 [6]
Littman	6.9	1.365 *	-	-	0.14	2016 [10]
Littman	4.46–4.75 *	0.29	20.8	25	0.2	2018 [11]
Littman	10.1–11.2	1.1 *	16	-	-	2018 [12]
AOM	4.44–5.02 *	0.58 *	14	-	-	2019 [17]
Intra-cavity out-coupling	8.4–10.8	2.4 *	1000	-	-	2021 [13]
MMI	8	0.391 *	1450	-	0.25	2021 [16]
Littrow	4.45–4.80	0.35	68	>20	-	2022 [7]
Littrow	4.33–4.87	0.54	70	20–70	0.001	2022 [8]

Note: "\*" denotes that the data are calculated, "-" denotes that the data are not available.

#### 4. Applications of Mid-Infrared ECQCLs

ECQCLs have the advantages of high conversion efficiency, compact size, and high reliability [18]. Their lasing wavelength covers two important atmospheric windows of 3–5  $\mu\text{m}$  and 8–14  $\mu\text{m}$ ; thus, it can be used in molecular detection, free space communication, and industry applications. Using tunable ECQCL spectroscopy has many advantages, including high sensitivity and selectivity. It is non-destructive, fast, and requires no sample preparation. With advances in ECQCLs in terms of tunability, output power, reliability, and operating temperature, there has been a growing interest in the use of ECQCLs for gas detection by spectroscopic groups. Molecular detection is currently the most studied and widely used field, such as environmental monitoring, emission measurement, remote sensing, medical and life science applications [19], industrial process control, safety, and basic science, all of which benefit from the technological advancements in ECQCLs. Different techniques for absorption spectroscopy were demonstrated using ECQCLs [20,21]. Various substances have unique functional groups, and specific functional groups have specific optical activities and have different absorption characteristics for different wavelength lasers. Therefore, by analyzing the spectral changes caused by the gas, the corresponding molecular content and species can be obtained. Due to the high resolution and high reliability of ECQCLs, there are important application prospects in this field. Laser-based infrared spectroscopy is an emerging key technology for analyzing solutes and monitoring reactions in liquids in real time. Compared to the traditional standard Fourier transform infrared spectroscopy (FTIR), the larger applicable path length enables the robust measurement of analytes in strongly absorbing matrices such as water. Recent advances in laser development have also provided a wide range of accessible spectral coverage, thus overcoming the inherent shortcomings of laser-based infrared spectroscopy.

##### 4.1. Application of ECQCLs in Gas Detection

The detection of gas is important in many applications, including combustion diagnostics, industrial detection, atmospheric detection, and medical detection.

###### 4.1.1. Nitric Oxide (NO) Detection

In 2005, G. Wysocki et al. [22] reported a mode-hopping, broadly tunable CW and thermoelectrically cooled ECQCL capable of high-resolution spectroscopic measurements. The

system provides independent wavelength tracking through all three wavelength-selective elements of ECQCLs, which made it suitable for applications using gain chips. The current prototype instrument had a wavelength of  $5.2 \mu\text{m}$ , a tuning range of  $35 \text{ cm}^{-1}$ , and a continuous mode-hop-free (MHF) mode tuning range of  $2 \text{ cm}^{-1}$ . The overall performance of the spectrometer system was demonstrated by direct absorption spectroscopy measurements of NO under reduced pressure. Its wavelength modulation capability, coupled with wide tunability and high spectral resolution, made the ECQCL an excellent light source for many mid-infrared spectroscopy applications, such as trace gas detection.

In 2010, V. Spagnolo et al. [23] reported a gas sensor based on quartz-enhanced photoacoustic detection and an ECQCL. It was characterized by NO absorption multiplication at  $5.26 \mu\text{m}$  to monitor trace NO and studied the dependence of signal and noise on gas pressure to optimize the performance of the sensor. The tuning range of the ECQCL was  $5.13\text{--}5.67 \mu\text{m}$ , and the specified MHF mode tuning range was  $5.26\text{--}5.53 \mu\text{m}$ , which corresponded to 5% of its central wavelength; the output power exceeded 100 mW. By contrast, quartz-enhanced photoacoustic spectroscopy (QEPAS) technology was competitive in sensitivity, while offering a more compact sensor design and smaller size.

#### 4.1.2. CO<sub>2</sub> Detection

In 2017, Ramin Ghorbani et al. [24] reported a mid-infrared tunable diode laser absorption spectroscopy sensor for the real-time detection of CO<sub>2</sub> in exhaled breath. The system used an ECQCL. The output wavelength tunable range was from  $4.50$  to  $4.96 \mu\text{m}$ , and the peak output power was 160 mW.

#### 4.1.3. Butane (C<sub>4</sub>H<sub>10</sub>) Detection

In 2013, D. Mammez et al. [25] reported the commercialization of an ECQCL in a photoacoustic spectrometer with an emission wavelength of  $10.5 \mu\text{m}$ . The spectrometer could measure in a wide spectral range of  $60 \text{ cm}^{-1}$ , which means that the spectra of complex molecules as well as the entire absorption bands of small molecules could be recorded. The wide tuning range of this photoacoustic spectrometer light source demonstrates the possibility of detecting complex small molecules such as CO<sub>2</sub> and C<sub>4</sub>H<sub>10</sub>. Figure 9 shows the structure diagram of spectral detection.

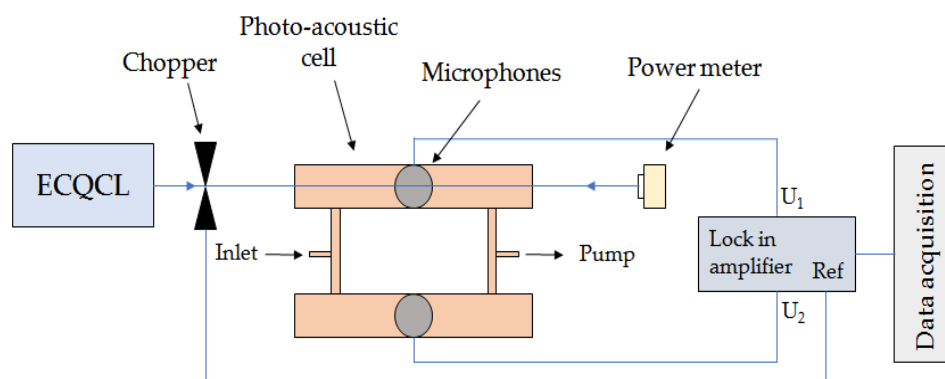


**Figure 9.** Structure diagram of spectral detection.

#### 4.1.4. Acetylene (C<sub>2</sub>H<sub>2</sub>) Detection

In 2018, Abhijit Maity et al. [26] reported a mid-infrared detection strategy using an ECQCL, and the working wavelength was from  $7.5 \mu\text{m}$  to  $8 \mu\text{m}$ . The C<sub>2</sub>H<sub>2</sub> detection had a noise limit of three parts per billion (ppb), and the integration time was 110 s. The current high resolution ECQCL system was further validated in the C<sub>2</sub>H<sub>2</sub> concentration range of 0.1–1000 ppm, which showed good promise in practical sensing applications.

#### 4.1.5. Nitrous Oxide(N<sub>2</sub>O) Detection

In 2019, Faisal Nadeem et al. [27] reported a mid-infrared trace gas detection system that was used to detect N<sub>2</sub>O. An ECQCL was used in the system, and the working wavelength was 7.7 μm, the output power was 40 mW, and the tunable range was about 320 cm<sup>-1</sup>.

#### 4.1.6. Methane (CH<sub>4</sub>) Detection

In 2017, Abhijit Maity et al. [28] reported mid-infrared CW cavity ring down spectroscopy (CRDS) technology and MHF ECQCL technology operating at 7.5 μm. The authors validated the ECQCL-based high-resolution CW-CRDS system by measuring the <sup>12</sup>CH<sub>4</sub> and <sup>13</sup>CH<sub>4</sub> isotopes of CH<sub>4</sub> as a reference molecule. By probing the asymmetric bending (ν<sub>4</sub> band), vibrations of the <sup>12</sup>C and <sup>13</sup>C isotopes of CH<sub>4</sub> in the sample from bonds centered at 7.534 μm and 7.502 μm, respectively. The current high-resolution CW-CRDS system could further utilize the spectral region covering 7.5–8 μm to trace several other molecular species and their isotopes.

In 2018, Xiaojuan Cui et al. [29] introduced a compact laser absorption sensor system associated with a 152 m long absorption cell for the simultaneous detection of N<sub>2</sub>O, CH<sub>4</sub>, and the second harmonic of H<sub>2</sub>O vapor. An 8 μm ECQCL was the excitation laser source, and three adjacent absorption lines, N<sub>2</sub>O, CH<sub>4</sub>, and H<sub>2</sub>O, at 7.968 μm and 7.969 μm were simultaneously aimed at 7.965 μm. At the optimum pressure of 50 Torr, the lowest detection limit was achieved with 1 s integration time, 0.9 ppb for N<sub>2</sub>O, 4.8 ppb for CH<sub>4</sub>, and 31 ppm for H<sub>2</sub>O.

In 2021, Qianhe Wei et al. [30] reported a gas sensor based on a tunable 7.6 μm CW MHF ECQCL (from 7.4 μm to 7.7 μm) CRDS technique. The sensor could detect CH<sub>4</sub> and N<sub>2</sub>O in ambient air.

#### 4.1.7. Chlorodifluoromethane (CHClF<sub>2</sub>) Detection

CHClF<sub>2</sub> is one of the most abundant HCFCs in the atmosphere. Due to its relatively low ozone depletion potential in chlorine-containing haloalkanes, it is often used as a replacement for the high ozone depleting CFC-11 and CFC-12. CHClF<sub>2</sub> is commonly used as a refrigerant in air conditioning systems. Although developed countries are phasing out CHClF<sub>2</sub> due to high global warming potential, the use of CHClF<sub>2</sub> continues to increase due to a high demand in developing countries. In 2019, Sheng Zhou et al. [31] reported a sensor that used QEPAS and ECQCL to detect CHClF<sub>2</sub> with unresolved rotation-vibration absorption lines. The spectral range was from 7.04 μm to 8.13 μm.

#### 4.1.8. Hydrogen Sulfide (H<sub>2</sub>S) Detection

In 2017, Michal Nikodem et al. [32] reported on a quantum cascade laser-based spectroscopic system for the detection of H<sub>2</sub>S in the mid-infrared of 7.2 μm, and the wavelength tunable range was from 7 to 8.2 μm.

In 2019, Mithun Pal et al. [33] reported a sensor that used a mid-infrared ECQCL cavity ring-down spectroscopy to simultaneously monitor the <sup>32</sup>S, <sup>33</sup>S, and <sup>34</sup>S isotopes of H<sub>2</sub>S. It verified the possibility of this system for tracking the characteristics of sulfur isotopes in compounds in practical applications. Nine independent transition lines of H<sub>2</sub><sup>32</sup>S and H<sub>2</sub><sup>33</sup>S isotopes in the current MHF ECQCL tuning range were further explored for the trace monitoring of the H<sub>2</sub>S single isotope. At a pressure of 30 Torr and an integration time of 255 s, the lowest detection limit was 20 ppb. It provided a new method that combined the unique spectral features of 7.5 μm, the high sensitivity of CRDS technology, the high resolution of ECQCL, and a wide MHF tunability.

#### 4.1.9. Sulfur Dioxide (SO<sub>2</sub>)

In 2020, Xukun Yin et al. [34] reported a ppb-level SO<sub>2</sub> photoacoustic sensor using a 7.41 μm ECQCL to suppress the absorption-desorption effect. For the first time, a CW ECQCL combined with a customized differential photoacoustic cell was employed to detect trace SO<sub>2</sub> in mid-infrared. The ECQCL current was set at 700 mA and operated in MHF

mode. The maximum power was about 60 mW in the wavelength between 7.35  $\mu\text{m}$  and 7.45  $\mu\text{m}$ , satisfying the excitation wavelength requirement. When the input current was greater than 600 mA, the ECQCL started to emit light. Subsequently, the ECQCL output power with the large inner diameter of the two resonators and the differential photoacoustic cell structure could reduce the background noise and response time, resulting in the best detection limit at the ppb level.

#### 4.1.10. Benzene ( $\text{C}_6\text{H}_6$ ) Detection

In 2020, Mohammad Khaled Shakfa et al. [35] reported a new mid-infrared laser diagnostic instrument for  $\text{C}_6\text{H}_6$  measurement. The structure is shown in Figure 10, and this instrument consisted of an ECQCL and a  $\text{CO}_2$  gas laser, directional patterned GaAs crystal. The laser system emitted a laser that ranged from 12.64  $\mu\text{m}$  to 15  $\mu\text{m}$  in the mid-infrared region. The laser was tuned to the Q-branch transition peak around 14.838  $\mu\text{m}$ , and it showed that the cross section of  $\text{C}_6\text{H}_6$  was very sensitive to pressure. Experiments were carried out after reflecting the shock wave to determine the absorption cross section of  $\text{C}_6\text{H}_6$  at 553–1473 K and 1.17–2.48 bar. This new detection method was been confirmed in the reaction shock tube experiment of propargyl iodide to  $\text{C}_6\text{H}_6$ .

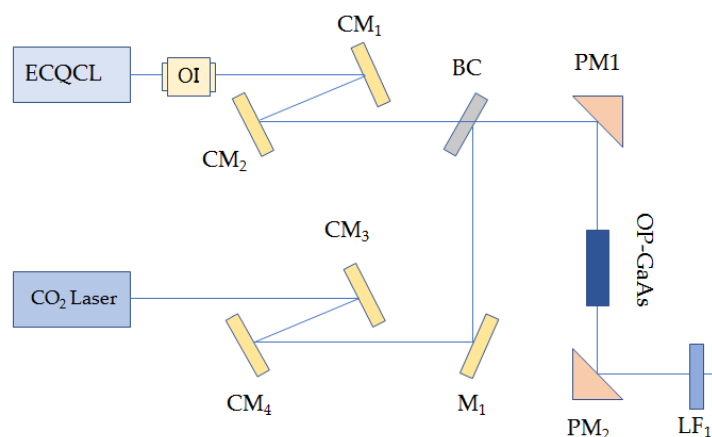


**Figure 10.** Schematic drawing of the mid-infrared laser setup.

#### 4.1.11. Volatile Organic Compounds (VOCs) Detection

Ethanol and acetone are the most common VOCs, are good organic solvents in plastics, rubber, paint, and other industries, and are also commonly used detergents in laboratories [36]. However, continued exposure to these VOCs can lead to feelings of irritation, many other uncomfortable symptoms, and even the risk of cancer, and VOCs readily react with atmospheric oxidants, leading to ozone pollution and atmospheric acidification. Therefore, studying the real-time monitoring of VOCs is crucial for optimizing the living environment and protecting human health.

In 2016, Juan Sun et al. [37] reported a tunable diode laser absorption spectroscopy system based on a broad band ECQCL near 7.78  $\mu\text{m}$  that was used to study VOC measurements. The tunable wavelength range of the ECQCL was from 6.96  $\mu\text{m}$  to 8.85  $\mu\text{m}$ .

In 2018, Ningwu Liu et al. [38] reported a broadband ECQCL-based sensor used for the open-path sensing of multiple VOCs. The ECQCL had a tuning range of 6.96–8.85  $\mu\text{m}$ , and the laser could generate different pulse repetition rates (up to 3 MHz) in the pulse range from 20 ns to 350 ns while maintaining a duty cycle of about 15%. The ECQCL sensor was successfully used for the long-range detection of mixed plumes of three VOCs at a distance of 40 m, proving its suitability for leak plumes in the safety field. Preliminary alcohol, acetone, ether open circuit detection, and identification tests demonstrated the high potential of the ECQCL sensor for monitoring chemical leaks in the safety field.

#### 4.1.12. Alkanes Detection

In 2019, Robet Heinrich et al. [39] reported a multi-component spectrum of hydrocarbons based on a CW ECQCL spectrometer, which provided a tunability of 6–11  $\mu\text{m}$  to measure the first seven alkanes and their mixtures. Gas spectra were obtained in the range 6.756–6.944  $\mu\text{m}$  at a reduced pressure of 50 mbar and a temperature of 323 K. Spectral accuracy up to  $\pm 0.001\text{ cm}^{-1}$  was achieved by the linearization of the measurement wavelength using a custom made highly temperature-stabilized air spaced etalon. The high resolution of  $0.001\text{ cm}^{-1}$  produced heavy alkane ( $\text{C}_3\text{--C}_5$ ) spectra with unprecedented richness details and allowed to distinguish narrow spectral features of light alkanes ( $\text{C}_1\text{--C}_2$ ).

#### 4.2. Protein Detection

Due to the limited emission wavelength range of ECQCLs, the spectral coverage is limited compared to FTIR, but its significant advantage is that it is stable and convenient in the detection of amides [40]. The large optical path can be used to directly measure the infrared absorption spectrum of water-based solutions, such as body fluids (blood, serum, breast milk), foods (commercial milk), etc. Compared to earlier laser-based infrared lasers, the expanded spectral coverage, including the most prominent protein infrared band, provides advantages for qualitative and quantitative studies of proteins. In the future, ECQCLs will be used to study dynamic secondary structure changes and stoichiometry-based protein quantification in complex matrices.

In 2019, Milagros Montermurro et al. [41] reported a rapid analysis system of commercial milk proteins using ECQCL mid-infrared spectroscopy. In the system, a thermoelectrically cooled ECQCL with a repetition rate of 100 kHz and a pulse width of 5000 ns was used. All spectra were recorded in the spectral tuning range of 5.78–6.8  $\mu\text{m}$ , covering the amide I and amide II regions of the protein, with a scan speed of  $1200\text{ cm}^{-1}\text{s}^{-1}$ . The mid infrared ECQCL was focused on the detector element by a gold-coated off-axis parabolic mirror with a focal length of 43 mm. The operating temperature was  $-78\text{ }^\circ\text{C}$ .

In 2020, Alicja Dabrowska et al. [42] reported a Mach-Zehnder interferometer-based sensor for detecting the dispersive spectroscopy of proteins. This is also the first time that the refractive index spectrum of a protein was measured with such high speed and resolution over such a broad spectral range. The thermoelectrically cooled ECQCL could be tuned in the range of 5.78–6.8  $\mu\text{m}$ . Dispersive spectroscopy achieves a figure of merit similar to established high-end FTIR spectroscopy at the same acquisition time. In the same year, a mid-infrared transmission setup for the analysis of protein amide I and amide II bands in aqueous solution was studied using the ECQCL.

In 2021, Schwaighofer Andreas et al. [43] reported a commercial room temperature operating broadband ECQCL infrared spectroscopy with a spectral coverage of 5.65–7.4  $\mu\text{m}$  combined with FTIR spectroscopy that was compared and demonstrated for its application in measuring a protein secondary structure in water and for monitoring the lipase-catalyzed saponification of triacetin. For the obtained limits of detection, ECQCL-based spectrometers performed better than research-grade FTIR spectrometers with liquid nitrogen cooled detectors. The device monitored the enzymatic hydrolysis of triacetin by lipase, demonstrating the advantage of broad spectral coverage for the subsequent monitoring of complex chemical reactions that cannot be readily obtained by FTIR spectroscopy without the use of liquid nitrogen cooling.

#### 4.3. Industry Detection

In 2020, Mark C. Phillips et al. [44] reported a swept-wavelength ECQCL that was used to perform the standoff detection of combustion gases in a plume generated from an outdoor high-explosive open detonation. The swept-ECQCL system was located at a standoff distance of 830 m from a 41 kg charge of LX-14 (polymer-bonded high explosive) and was used to measure the infrared transmission or absorption through the post-detonation plume as it propagated through the beam path. The swept-ECQCL was operated continuously to record broadband absorption spectra at a 200 Hz rate over a spectral range from  $2050\text{ cm}^{-1}$

to  $2230\text{ cm}^{-1}$ . The fitting of measured spectra was used to determine time-resolved column densities of CO, CO<sub>2</sub>, H<sub>2</sub>O, and N<sub>2</sub>O.

In 2020, Anaïs Parrot et al. [45] reported an ECQCL mid-infrared reflectance spectroscopy that was used to discriminate silicate and carbonate minerals in a standoff measurement setting. The tunable ECQCL source that was used allowed measurement from the 5.2  $\mu\text{m}$  to 13.4  $\mu\text{m}$  wavelength, where the fundamental vibrational bands of silicates and carbonates were observed. Mid-infrared reflectance spectroscopy using compact ECQCL sources allowed rapid spectral measurements at standoff distances and high spatial resolution. It showed the potential of ECQCL mid-infrared reflectance spectroscopy for in the field mining applications.

In 2022, Francis Vanier et al. [46] designed an ECQCL-based mid-infrared spectrometer. The light source consisted of four ECQCLs with spectral coverage ranging from 5.2  $\mu\text{m}$  to 13.4  $\mu\text{m}$  wavelengths. The performance of a mid-infrared reflectance spectroscopy device based on a tunable ECQCL module was described. The results assessed the quality and usability of spectra of mineral mixtures obtained using ECQCL-based mid-infrared spectroscopy, completing the first step in mineral characterization using ECQCL-based mid-infrared spectroscopy.

The research development on applications of ECQCLs in recent years is listed in Table 2. The recent availability of ECQCLs provides a promising new avenue for multi-component detection and protein detection. Based on the recent development of advanced instrumentation, including compact and robust ECQCL systems, the promotion of this high resolution mid-infrared spectroscopy for industrial applications has been rapidly realized.

**Table 2.** The applications of ECQCLs and the detection substance.

$\lambda$ ( $\mu\text{m}$ )	Tuning Range ( $\mu\text{m}$ )	Detect Matter	Application Field	Year
5.2	0.09 *	NO	Gas detection	2005 [22]
5.26	0.54 *	NO	Gas detection	2010 [23]
10.5	0.62 *	C <sub>4</sub> H <sub>10</sub>	Gas detection	2013 [25]
7.78	1.89	VOCs	Gas detection	2016 [37]
4.50–4.96	0.46	CO <sub>2</sub>	Gas detection	2017 [24]
7.2	1.2	H <sub>2</sub> S	Gas detection	2017 [32]
7.5–8	0.5	CH <sub>4</sub>	Gas detection	2017 [28]
7.5–8	0.5	C <sub>2</sub> H <sub>2</sub>	Gas detection	2018 [26]
7.91–8.17 *	0.26 *	CH <sub>4</sub>	Gas detection	2018 [29]
6.96–8.85	1.89	VOCs	Gas detection	2018 [38]
7.7	1.92 *	NO <sub>2</sub>	Gas detection	2019 [27]
7.04–8.13 *	1.09 *	CHClF <sub>2</sub>	Gas detection	2019 [31]
7.46–7.95 *	0.49 *	H <sub>2</sub> S	Gas detection	2019 [33]
6–11	5	Alkane	Gas detection	2019 [39]
5.78–6.80 *	1.02 *	Milk	Protein detection	2019 [41]
7.20–7.52	0.32	SO <sub>2</sub>	Gas detection	2020 [34]
12.64–15.00 *	2.36 *	C <sub>6</sub> H <sub>6</sub>	Gas detection	2020 [35]
5.78–6.80 *	1.02 *	Protein	Protein detection	2020 [42]
4.48–4.88	0.4	Explosives	Industry detection	2020 [44]
5.2–13.4	8.2	Silicate and carbonate minerals	Industry detection	2020 [45]
7.40–7.75 *	0.35 *	CH <sub>4</sub>	Gas detection	2021 [30]

Table 2. Cont.

$\lambda$ ( $\mu\text{m}$ )	Tuning Range ( $\mu\text{m}$ )	Detect Matter	Application Field	Year
5.64–7.40 *	1.76 *	Protein, Enzymatic activity	Protein detection	2021 [43]
5.2–13.4	8.2	Mineral	Industry detection	2022 [46]

Note: “\*” denotes that the data are calculated.

## 5. Summary

In the field of mid-infrared ECQCL laser research [47], several open questions invite major research investment. Such fundamental issues include the development of sub-picosecond ECQCLs, high-pulse-energy pulsed ECQCLs, ECQCLs used to detect materials, and ECQCLs used as consumer electronics. Such devices would highlight the significant potential of ECQCLs and open up new fields for research and applications.

Mid-infrared techniques are a very powerful tool for molecular spectroscopy because many molecular vibrational modes lie in this wavelength range [48,49]. An ECQCL is a mid-infrared tunable ECQCL that can cover any part of this spectral range. Therefore, ECQCLs have great application potential as industrial-scale standard light sources.

After more than 20 years of rapid development, QCLs are becoming the most important mid-far-infrared light sources [50]. The advantages of QCLs are vividly reflected in the fields of high-power devices, low-power single mode devices, high-speed tunable devices, and broadband optical frequency comb devices. In the near future, quantum cascade lasers will play an increasingly important role in infrared countermeasures, gas sensing, and free space communication. With the continuous optimization of the external cavity structure, ECQCLs will bring a wider tuning range and narrower linewidth in the future, which will shine in environmental monitoring, medical treatment, infrared countermeasures, etc.

**Author Contributions:** Conceptualization, Y.M., Z.L. and K.D.; methodology, X.L. and J.S.; writing—original draft preparation, X.L. and Z.L.; writing—review and editing, L.W., L.L. and L.Z.; visualization, G.L. and Y.Q.; supervision, Z.Q. and D.X.; funding acquisition, G.L. All authors have read and agreed to the published version of the manuscript.

**Funding:** This work was supported in part by a specific research fund for the Innovation Platform for Academicians of Hainan Province under Grant YSPTZX202034 and Grant YSPTZX202127; in part by the Major Science and Technology Program of Hainan Province of China under Grant ZDKJ 2019005; in part by Scientific Research Projects of Higher Education Institutions in Hainan Province under Grant hnky2020-24, Grant Hnjg2021ZD-22, Grant hnky2020ZD-12; in part by the Hainan Provincial Natural Science Foundation of China under Grant 622RC671, Grant 120MS031, Grant 2019RC190, Grant 2019RC192; in part by the National Natural Science Foundation of China under Grant 61774024, Grant 61864002, Grant 11764012, Grant 62174046, Grant 62064004 and Grant 61964007; in part by the Key Research and Development Projects in Hainan Province under Grant ZDYF2020020, Grant ZDYF2020036, and Grant ZDYF2020217; in part by the Open Fund for Innovation and Entrepreneurship of college students under Grant 202111658021X, Grant 202111658022X, Grant 202111658023X, Grant 202111658013.

**Data Availability Statement:** Not applicable.

**Acknowledgments:** The authors thank Hao Chen, Yanbo Liang, and Xing Mu for helping with this article.

**Conflicts of Interest:** Not applicable.

## References

1. Capasso, F. High-performance mid-infrared quantum cascade lasers. *Opt. Eng.* **2010**, *49*, 1102. [CrossRef]
2. Maulini, R.; Mohan, A.; Giovannini, M.; Faist, J.; Gini, E. External cavity quantum-cascade laser tunable from 8.2 to 10.4  $\mu\text{m}$  using a gain element with a heterogeneous cascade. *Appl. Phys. Lett.* **2006**, *88*, 2834–2883. [CrossRef]

3. Wysocki, G.; Weidmann, D. Applications of external cavity quantum cascade lasers: Broadband mid-IR laser heterodyne radiometry. In Proceedings of the Conference on Lasers and Electro-Optics, Optical Society of America, Baltimore, MD, USA, 31 May–5 June 2009.
4. Mammez, D.; Vallon, R.; Parvitte, B.; Mammez, M.-H.; Carras, M.; Zéninari, V. Development of an external cavity quantum cascade laser spectrometer at 7.5  $\mu\text{m}$  for gas detection. *Appl. Phys. A* **2014**, *116*, 951–958.
5. Xie, F.; Caneau, C.; Leblanc, H.; Ho, M.T.; Zah, C. Ultra-broad gain quantum cascade lasers tunable from 6.5 to 10.4  $\mu\text{m}$ . *Opt. Lett.* **2015**, *40*, 4158–4161. [[CrossRef](#)]
6. Zhao, Z.; Wang, L.; Jia, Z.; Zhang, J.; Liu, F.; Zhuo, N.; Zhai, S. Low-threshold external-cavity quantum cascade laser around 7.2  $\mu\text{m}$ . *Opt. Eng.* **2016**, *55*, 046116. [[CrossRef](#)]
7. Bayrakli, I. Optically and electrically pumped grating-coupled external cavity quantum cascade laser. *Opt. Quantum Electron.* **2022**, *54*, 1–7. [[CrossRef](#)]
8. Bayrakli, I. External cavity quantum cascade lasers without anti-reflection coating with intra-cavity and extra-cavity acoustic-optic frequency shifter for fast standoff detection. *Opt. Laser Technol.* **2022**, *148*, 107747. [[CrossRef](#)]
9. Luo, G.; Peng, C.; Le, H.; Pei, S.-S.; Lee, H.; Hwang, W.-Y.; Ishaug, B.; Zheng, J. Broadly Wavelength-Tunable External Cavity Mid-Infrared Quantum Cascade Lasers. *IEEE J. Quantum Electron.* **2002**, *38*, 486–494.
10. Wei, L.; Chuan-Xi, D. A broadband pulsed external-cavity quantum cascade laser operating near 6.9  $\mu\text{m}$ . *Chin. Phys. Lett.* **2016**, *33*, 024207. [[CrossRef](#)]
11. Jia, X.; Wang, L.; Jia, Z.; Zhuo, N.; Zhang, J.; Zhai, S.; Liu, J.; Liu, S.; Liu, F.; Wang, Z. Fast Swept-Wavelength, Low Threshold-Current, Continuous-Wave External Cavity Quantum Cascade Laser. *Nanoscale Res. Lett.* **2018**, *13*, 341. [[CrossRef](#)]
12. Dougakiuchi, T.; Kawada, Y.; Takebe, G. Continuous multispectral imaging of surface phonon polaritons on silicon carbide with an external cavity quantum cascade laser. *Appl. Phys. Express* **2018**, *11*, 032001. [[CrossRef](#)]
13. Matsuoka, Y.; Peters, S.; Semtsiv, M.P.; Masselink, W.T. External-cavity quantum cascade laser using intra-cavity out-coupling. *Opt. Lett.* **2018**, *43*, 3726–3729. [[CrossRef](#)] [[PubMed](#)]
14. Zhou, W.; Slivken, S.; Razeghi, M. Phase-locked, high power, mid-infrared quantum cascade laser arrays. *Appl. Phys. Lett.* **2018**, *112*, 181106. [[CrossRef](#)]
15. Zhou, W.; Wu, D.; Lu, Q.-Y.; Slivken, S.; Razeghi, M. Single-mode, high-power, mid-infrared, quantum cascade laser phased arrays. *Sci. Rep.* **2018**, *8*, 14866. [[CrossRef](#)]
16. Gu, Z.-H.; Zhang, J.-C.; Wang, H.; Yang, P.-C.; Zhuo, N.; Zhai, S.-Q.; Liu, J.-Q.; Wang, L.-J.; Liu, S.-M.; Liu, F.-Q.; et al. Tunable characteristic of phase-locked quantum cascade laser arrays. *Chin. Phys. B* **2021**, *30*, 104201. [[CrossRef](#)]
17. Lyakh, A.; Azim, A.; Loparo, Z.E.; Thurmond, K.; Vasu, S.S. Design of External Cavity Quantum Cascade Lasers for Combustion and Explosion Diagnostics. In Proceedings of the 2019 IEEE Research and Applications of Photonics in Defense Conference (RAPID), Miramar Beach, FL, USA, 19–21 August 2019.
18. Niu, S.; Liu, J.; Zhang, J.; Zhuo, N.; Zhai, S.; Wang, X.; Wei, Z. Single-Mode Fabry-Pérot Quantum Cascade Lasers at  $\lambda \sim 10.5 \mu\text{m}$ . *J. Mater. Sci. Chem. Eng.* **2020**, *8*, 85–91.
19. Risby, T.; Solga, S. Current status of clinical breath analysis. *Appl. Phys. A* **2006**, *85*, 421–426.
20. Wysocki, G.; Lewicki, R.; Curl, R.; Tittel, F.; Diehl, L.; Capasso, F.; Troccoli, M.; Höfler, G.; Bour, D.; Corzine, S.; et al. Widely tunable mode-hop free external cavity quantum cascade lasers for high resolution spectroscopy and chemical sensing. *Appl. Phys. B* **2008**, *92*, 305–311. [[CrossRef](#)]
21. Kosterev, A.; Wysocki, G.; Bakhirkin, Y.; So, S.; Lewicki, R.; Fraser, M.; Tittel, F.; Curl, R. Application of quantum cascade lasers to trace gas analysis. *Appl. Phys.* **2008**, *690*, 165–176. [[CrossRef](#)]
22. Wysocki, G.; Curl, R.; Tittel, F.; Maulini, R.; Bulliard, J.; Faist, J. Widely tunable mode-hop free external cavity quantum cascade laser for high resolution spectroscopic applications. *Appl. Phys. B* **2005**, *81*, 769–777. [[CrossRef](#)]
23. Spagnolo, V.; Kosterev, A.A.; Dong, L.; Lewicki, R.; Tittel, F.K. NO trace gas sensor based on quartz-enhanced photoacoustic spectroscopy and external cavity quantum cascade laser. *Appl. Phys. B* **2010**, *100*, 125–130. [[CrossRef](#)]
24. Ramin, G.; Schmidt, F.M. Real-time breath gas analysis of CO and CO<sub>2</sub> using an EC-QCL. *Appl. Phys. B* **2017**, *123*, 144.
25. Mammez, D.; Stoeffler, C.; Cousin, J.; Vallon, R.; Mammez, M.; Joly, L.; Parvitte, B.; Zéninari, V. Photoacoustic gas sensing with a commercial external cavity-quantum cascade laser at 10.5  $\mu\text{m}$ . *Infrared Phys. Technol.* **2013**, *61*, 14–19. [[CrossRef](#)]
26. Maity, A.; Pal, M.; Maithani, S.; Banik, G.D.; Pradhan, M. Wavelength modulation spectroscopy coupled with an external-cavity quantum cascade laser operating between 7.5 and 8  $\mu\text{m}$ . *Laser Phys. Lett.* **2018**, *15*, 045701. [[CrossRef](#)]
27. Nadeem, F.; Khodabakhsh, A.; Mandon, J.; Cristescu, S.S.; Harren, F.J.M. Detection of N<sub>2</sub>O Using An External-Cavity Quantum Cascade Laser. *OSA Contin.* **2019**, *2*, 2667–2682. [[CrossRef](#)]
28. Maity, A.; Pal, M.; Banik, G.D.; Maithani, S.; Pradhan, M. Cavity ring-down spectroscopy using an EC-QCL operating at 7.5  $\mu\text{m}$  for direct monitoring of methane isotopes in air. *Laser Phys. Lett.* **2017**, *14*, 115701. [[CrossRef](#)]
29. Cui, X.; Dong, F.; Zhang, Z.; Sun, P.; Xia, H.; Fertein, E.; Chen, W. Simultaneous detection of ambient methane, nitrous oxide, and water vapor using an external-cavity quantum cascade laser. *Atmos. Environ.* **2018**, *189*, 125–132. [[CrossRef](#)]
30. Wei, Q.; Li, B.; Wang, J.; Zhao, B.; Yang, P. Impact of Residual Water Vapor on the Simultaneous Measurements of Trace CH<sub>4</sub> and N<sub>2</sub>O in Air with Cavity Ring-Down Spectroscopy. *Atmosphere* **2021**, *12*, 221. [[CrossRef](#)]
31. Zhou, S.; Xu, L.; Zhang, L.; He, T.; Liu, N.; Liu, Y.; Yu, B.; Li, J. External cavity quantum cascade laser-based QEPAS for chlorodifluoromethane spectroscopy and sensing. *Appl. Phys. B* **2019**, *125*, 125. [[CrossRef](#)]

32. Nikodem, M.; Krzempek, K.; Stachowiak, D.; Wysocki, G. Quantum cascade laser-based analyzer for hydrogen sulfide detection at sub-parts-per-million levels. *Opt. Eng.* **2017**, *57*, 011019. [[CrossRef](#)]
33. Pal, M.; Maithani, S.; Maity, A.; Pradhan, M. Simultaneous monitoring of  $^{32}\text{S}$ ,  $^{33}\text{S}$  and  $^{34}\text{S}$  isotopes of  $\text{H}_2\text{S}$  using cavity ring-down spectroscopy with a mid-infrared external-cavity quantum cascade laser. *J. Anal. At. Spectrom.* **2019**, *34*, 860–866. [[CrossRef](#)]
34. Yin, X.; Wu, H.; Dong, L.; Li, B.; Ma, W.; Zhang, L.; Yin, W.; Xiao, L.; Jia, S.; Tittel, F.K. ppb-level  $\text{SO}_2$  photoacoustic sensors with a suppressed absorption-desorption effect by using a 7.41  $\mu\text{m}$  external-cavity quantum cascade laser. *ACS Sens.* **2020**, *5*, 549–556. [[CrossRef](#)] [[PubMed](#)]
35. Shakfa, M.K.; Mhanna, M.; Jin, H.; Liu, D.; Djebbi, K.; Marangoni, M.; Farooq, A. A mid-infrared diagnostic for benzene using a tunable difference-frequency-generation laser. *Proc. Combust. Inst.* **2021**, *38*, 1787–1796. [[CrossRef](#)]
36. Sun, J.; Ding, J.; Liu, N.; Yang, G.; Li, J. Detection of multiple chemicals based on external cavity quantum cascade laser spectroscopy. *Spectrochim. Acta Part A Mol. Biomol. Spectrosc.* **2018**, *191*, 532–538. [[CrossRef](#)]
37. Sun, J.; Liu, N.; Deng, H.; Ding, J.; Sun, J.; Zhang, L.; Li, J. Laser absorption spectroscopy based on a broadband external cavity quantum cascade laser. *Int. Conf. Opt. Photonics Eng. SPIE* **2017**, *10250*, 378–382.
38. Liu, N.; Zhou, S.; Zhang, L.; Yu, B.; Fischer, H.; Ren, W.; Li, J. Standoff detection of VOCs using external cavity quantum cascade laser spectroscopy. *Laser Phys. Lett.* **2018**, *15*, 085701. [[CrossRef](#)]
39. Heinrich, R.; Popescu, A.; Strzoda, R.; Hangauer, A.; Höfling, S. High resolution quantitative multi-species hydrocarbon gas sensing with a cw external cavity quantum cascade laser based spectrometer in the 6–11  $\mu\text{m}$  range. *J. Appl. Phys.* **2019**, *125*, 134501. [[CrossRef](#)]
40. Schwaighofer, A.; Montemurro, M.; Freitag, S.; Kristament, C.; Culzoni, M.J.; Lendl, B. Beyond FT-IR Spectroscopy EC-QCL based mid-IR Transmission Spectroscopy of Proteins in the Amide I and Amide II Region. *Anal. Chem.* **2018**, *90*, 7072–7079. [[CrossRef](#)]
41. Montemurro, M.; Schwaighofer, A.; Schmidt, A.; Culzoni, M.J.; Mayer, H.K.; Lendl, B. High-throughput quantitation of bovine milk proteins and discrimination of commercial milk types by external cavity-quantum cascade laser spectroscopy and chemometrics. *Analyst* **2019**, *144*, 5571–5579. [[CrossRef](#)]
42. Dabrowska, A.; Schwaighofer, A.; Lindner, S.; Lendl, B. Mid-IR refractive index sensor for detecting proteins employing an external cavity quantum cascade laser-based Mach-Zehnder interferometer. *Opt. Express* **2020**, *28*, 36632–36642. [[CrossRef](#)]
43. Schwaighofer, A.; Akhgar, C.K.; Lendl, B. Broadband laser-based mid-IR spectroscopy for analysis of proteins and monitoring of enzyme activity. *Spectrochim. Acta Part A Mol. Biomol. Spectrosc.* **2021**, *253*, 119563. [[CrossRef](#)] [[PubMed](#)]
44. Phillips, M.C.; Harilal, S.S.; Yeak, J.; Jason Jones, R.; Wharton, S.; Bernacki, B.E. Standoff detection of chemical plumes from high explosive open detonations using a swept-wavelength external cavity quantum cascade laser. *J. Appl. Phys.* **2020**, *128*, 163103. [[CrossRef](#)]
45. Parrot, A.; Vanier, F.; Blouin, A. Standoff mid-infrared reflectance spectroscopy using quantum cascade laser for mineral identification. *SPIE Future Sens. Technol.* **2020**, *11525*, 217–225.
46. Vanier, F.; Parrot, A.; Padioleau, C.; Blouin, A. Mid-Infrared Reflectance Spectroscopy Based on External Cavity Quantum Cascade Lasers for Mineral Characterization. *Appl. Spectrosc.* **2022**, *76*, 361–368. [[CrossRef](#)] [[PubMed](#)]
47. Yao, Y.; Hoffman, A.J.; Gmachl, C.F. Mid-infrared quantum cascade lasers. *Nat. Photonics* **2012**, *6*, 432–439. [[CrossRef](#)]
48. Miczuga, M.; Kopczyński, K. Application of cascade lasers to detection of trace gaseous atmospheric pollutants. *Laser Technol. Prog. Appl. Lasers. SPIE* **2016**, *10159*, 295–300.
49. Tittel, F.K.; Dong, L.; Lewicki, R.; Liu, K.; Spagnolo, V. Mid-infrared quantum cascade laser based trace gas technologies: Recent progress and applications in health and environmental monitoring. In Proceedings of the 2011 International Quantum Electronics Conference (IQEC) and Conference on Lasers and Electro-Optics (CLEO) Pacific Rim Incorporating the Australasian Conference on Optics, Lasers and Spectroscopy and the Australian Conference on Optical Fibre Technology, Sydney, Australia, 28 August–1 September 2011.
50. Almond, N.W.; Qi, X.; Degl’Innocenti, R.; Kindness, S.J.; Michailow, W.; Wei, B.; Braeuninger-Weimer, P.; Hofmann, S.; Dean, P.; Indjin, D.; et al. External cavity terahertz quantum cascade laser with a metamaterial/graphene optoelectronic mirror. *Appl. Phys. Lett.* **2020**, *117*, 041105. [[CrossRef](#)]